Electrochemical Zero Mode Waveguide Potential-Dependent Fluorescence of Glutathione Reductase at Single Molecule Occupancy

Seol Baek[1], Donghoon Han[2], Seung-Ryong Kwon[3], Vignesh Sundaresan[4], and Paul W. Bohn[1,4*]

[1]Department of Chemistry and Biochemistry, University of Notre Dame, Notre Dame, Indiana 46556, United States

[2]Department of Chemistry, The Catholic University of Korea, Bucheon, Gyeonggi-do 14662, South Korea

[3]Department of Chemistry and Research Institute of Natural Science, Gyeongsang National University, Jinju, 52828, South Korea

[4]Department of Chemical and Biomolecular Engineering, University of Notre Dame, Notre Dame, Indiana 46556, United States

[*]Author to whom correspondence should be addressed, pbohn@nd.edu

Abstract

Understanding functional states of individual redox enzymes is important, because electron transfer reactions are fundamental to life, and single enzyme molecules exhibit molecule-to-molecule heterogeneity in their properties, such as catalytic activity. Zero mode waveguides (ZMW) constitute a powerful tool for single molecule studies, enabling investigations of binding reactions up to the micromolar range, due to the ability to trap electromagnetic radiation in zeptoliter-scale observation volumes. Here, we report the potential-dependent fluorescence dynamics of single glutathione reductase (GR) molecules using a bimodal electrochemical ZMW (E-ZMW) where a single ring electrode-embedded in each of the nanopores of an E-ZMW array simultaneously serves to control electrochemical potential and to confine optical radiation within the nanopores. Here, the redox state of GR is manipulated using external potential control of the Au electrode in the presence of a redox mediator, methyl viologen (MV). Redox state transitions in GR are monitored by correlating electrochemical and spectroscopic signals from freely-diffusing MV/GR in 60 zL effective observation volumes at single GR molecule average pore occupancy, $\langle n \rangle \sim 0.8$. Fluorescence intensities decrease (increase) at reducing (oxidizing) potentials for MV due to the MV-mediated control of the GR redox state. The spectroelectrochemical response of GR to the enzyme substrate, *i.e.*, glutathione disulfide (GSSG), shows that GSSG promotes GR oxidation *via* enzymatic reduction. The capabilities of E-ZMWs to probe spectroelectrochemical phenomena in zL-scale confined environments show great promise for study of single enzyme reactions and can be extended to important technological applications, such as those in molecular diagnostics.

Keywords: zero mode waveguides; single enzyme molecules; glutathione reductase; redox mediator; fluorescence spectroscopy; nanopore arrays

Introduction

Individual molecules exhibit variable behavior as evidenced by multiple functional states, state-dependent kinetics, and static and dynamic disorder, associated with intrinsic conformational variations and intermolecular interactions. In particular, enzymes display a rich array of such behaviors, involving sequential functional/structural changes presenting multiple kinetic states depending on conformation and substrate affinity.[1-5] Furthermore, single molecule investigations are useful in understanding chemical/physical phenomena in cells, because copy numbers of critical enzymes can be quite small and thus exhibit fluctuations reflecting both intrinsic variability and *in situ* perturbations.[6] Therefore, single molecule experiments are necessary to provide accurate information on enzymatic kinetics, catalytic activities, and systemic response to environmental stresses in small probe volumes.[7, 8]

High sensitivity spectroscopic approaches developed over the last 2-3 decades have enabled molecular investigations in structures of limited dimensionality, revealing subpopulations with different properties, down to the single molecule level. The heterogeneity present in single molecule experiments can be compared to the results of ensemble measurements which report on averages over phenotypes. In addition, single molecule sensitivity, implemented in parallel over arrays of single molecules, can enable the detection of rare events which may be lost in ensemble measurements.[9-11] Among the strategies for high sensitivity studies of small collections of active molecules, redox cycling-based electrochemical detection is a powerful method to examine redox-active species due to the ability to follow redox behavior at very low levels.[12] This is made possible by the signal amplification which results from rapid, alternating oxidation and reduction of redox species confined in a nanogap electrochemical cell.[13-17] However, both the technical challenges of high precision fabrication at the nanometer length scale and limitations on the gain-bandwidth

product applicable to measuring electrochemical signals constitute major hurdles to realizing purely electrochemical single molecule measurements.[13, 15] One way to circumvent this problem is to convert electron transfer processes to photon emission events, since spectroscopic measurements can often be realized at the shot noise limit, accessing measurements with relatively high S/N ratios and with the prospect of obtaining spatially resolved information.[15, 18-20] For spectroscopic studies at the single molecule level, the molecule of interest should be confined in an observation volume at a concentration adequate to isolate a few copies of the molecule from the bulk solution. However, many enzymatic reactions occur in the micromolar concentration range, thus requiring ultrasmall, zL-scale, observation volumes for single molecule studies.

In this regard, zero-mode waveguides (ZMWs) represent a promising platform enabling single molecule studies at relatively high, μM, concentrations, by confining the optical radiation in a small, typically zL-scale, observation volume.[21-24] ZMWs are photonic nanostructures consisting of sub-wavelength sized holes in thin metal films which, under the right conditions, can efficiently confine optical radiation in zL-aL observation volumes. Furthermore, above a material- and geometry-dependent cut-off wavelength, the intensity of the optical field decays along the axial direction in the ZMW, consistent with an evanescent field. Due to the extremely small observation volumes, ZMWs allow single molecules to be isolated and observed at micromolar concentrations. Real-time optical signals on ZMW platforms[24, 25] have enabled single molecule studies of DNA sequencing,[26-28] RNA modification,[29, 30] enzymatic activity,[22, 31] protein-protein [32, 33] and ligand-protein interactions.[34] Extending this concept, our laboratory has developed a bimodal photonic-electrochemical nanoarchitecture, *i.e.,* the electrochemical ZMW (E-ZMW), in which a metal cladding layer serves simultaneously to confine the optical field and as a working electrode (WE) to control potentials. The characteristics of the E-ZMW have been successfully

characterized using potential-dependent fluorescence by correlating electrochemical and spectroscopic signals generated from single electron-transfer events.[35]

In the present work, we investigate the potential-dependent fluorescence dynamics of single molecules of glutathione reductase (GR) in E-ZMWs. GR is an oxidoreductase capable of catalyzing the reduction of glutathione disulfide (GSSG) and plays a key role in preventing oxidative stress in eukaryotic cells.[36, 37] Moreover, GR is a homodimer flavoenzyme possessing a single flavin adenine dinucleotide (FAD) cofactor per monomer, which is strongly fluorescent in the oxidized state (GR_{ox}), but nearly dark in the reduced state (GR_{red}), as mediated by the reaction, $FAD + 2H^+ + 2e^- \rightleftarrows FADH_2$.[38-41] Here, we explore the *in situ* fluorescence dynamics of GR under external potential control and in response to surrounding environmental perturbations in the vicinity of the enzymes in E-ZMWs, **Figure 1A**. Since direct, tunneling-mediated electron transfer to GR occurs infrequently due to the long distance between the redox active center of GR and the electrode surface, and the ineffective charge transport characteristics of the intervening amino acids,[42-45] an alternative strategy was utilized here, in which electron transfer is assisted by a mediator in order to manipulate the redox states of GR molecules located distal to the electrode.[44] Methyl viologen (MV) is an efficient electrochemical redox mediator between GR and the Au nanopore electrodes.[42, 43] Single ring electrode-embedded E-ZMWs were fabricated to perform electrochemical measurements to monitor GR enzymatic reactions controlled by external potentials in the presence of a redox mediator. In addition, the real-time fluorescence dynamics of GR was monitored by measuring the on/off fluorescence signals corresponding to interconversion between emitting and dark GR redox states under potential control. Further, GR fluorescence dynamics was characterized under a variety of reaction conditions, for example, different GSSG concentrations.

Experimental Section

Chemicals and Materials. Glutathione reductase (GR) from baker's yeast (*S. cerevisiae*), L-glutathione oxidized form (GSSG), potassium phosphate monobasic, potassium phosphate dibasic, potassium nitrate (KNO_3), methyl viologen (MV) dichloride hydrate, and sulfuric acid (H_2SO_4) were purchased from Sigma-Aldrich. Poly(dimethylsiloxane) (PDMS) monomer and curing agent were obtained from Dow Corning. Glass coverslips (Nexterion Uncoated High Performance 1.5H Coverslips, Glass D263) were purchased from Applied Microarrays. All electrolyte solutions for spectroelectrochemical measurements were prepared using deionized (DI) water obtained from a Millipore Milli-Q system ($\rho \sim 18.2$ MΩ cm). GR in PB solution was prepared by centrifuging (10,000 × g, for 10 min) the GR suspension (supplied in ammonium sulfate containing 0.1 mM dithiothreitol; DTT), separating the GR pellet, and adding an appropriate amount of reaction buffer, to avoid the interference of DTT with redox reactions on the gold electrode. Planar Au electrodes were prepared by depositing 100 nm-thick Au on pre-cleaned glass slides (Glass D, Applied Microarrays, Inc.), using an electron beam evaporator (Airco Temescal FC-1800).

Fabrication and Characterization of E-ZMW Devices. E-ZMWs were fabricated by following the previous methods reported by this laboratory[35, 46], as shown in **Figure S1**. In brief, a patterned Au layer was produced by photolithography and electron beam deposition of 100 nm-thick Au on pre-cleaned glass coverslips. Then, a 100 nm-thick silicon dioxide (SiO_2) layer was deposited as the top layer by plasma-enhanced chemical vapor deposition (PECVD, Unaxis 790, Plasma-Therm). Focused ion beam (FIB) milling (FEI-Helios Dual-beam FIB) was used to create nanopore arrays in the multilayers, *i.e.,* 80 μm × 80 μm with an interpore distance of 2 μm, and 2 arrays in total per device, resulting in 3362 pores. The E-ZMW structures were characterized using

scanning electron microscopy (SEM), with an accelerating voltage of 5 kV and an electron beam current of 0.1 nA.

Spectroelectrochemical Measurements. Cyclic voltammetry (CV) and multiple potential step experiments were performed using either CHI 750E or CHI 760E electrochemical workstation (CH Instruments, USA) in a three-electrode system with a Pt counter electrode (CE) and a Ag/AgCl reference electrode (RE) (Harvard Apparatus, USA). CVs were measured at scan rates of 50 or 100 mV s^{-1}. Fluorescence measurements were conducted on an Olympus IX71 wide-field epi-illumination microscope equipped with a 100× oil-immersion objective (1.45 NA, Olympus Corporation, Japan) with illumination at 458 nm, **Figure 1A**. An electron multiplying charge-coupled device (EMCCD) detector (Andor Technology, UK) was used to collect the resulting fluorescence signals (200 ms/frame). Typically, 5 pixel × 5 pixel area corresponding to 800 nm × 800 nm was defined as a region of interest (ROI) for a single nanopore, and the fluorescence intensity from single nanopores was obtained by averaging the signal counts over each ROI, as illustrated in **Figure 1B**.

Results and Discussion

Development and Characterization of E-ZMWs. E-ZMW devices were fabricated by a combination of photolithography, multilayered deposition, and FIB milling to produce highly-ordered, single ring Au electrode-embedded nanopore arrays, **Figure S1**. The nanopore arrays were structurally characterized by SEM imaging, **Figure 1C-E**. Each E-ZMW nanopore in the array consists of a 100 nm Au ring electrode/cladding layer topped with 100 nm SiO_2 on a glass coverslip. The nanopore array size is 80 μm × 80 μm with 2 μm interpore distance, and the FIB-

milled pores are conical-shaped with top and bottom diameters of 110 and 80 nm, respectively, producing a single pore volume of *ca.* 1.8 aL (1 aL = 10^{-18} L). In the ZMW, the optical field decays exponentially along the axis of the nanopore, **Figure 1A**, when the incident wavelength is greater than a critical cutoff wavelength, $\lambda_c \sim 1.7d$, where d is the pore diameter, resulting in an observation volume occupying only a fraction of the geometric ZMW volume.[22] The effective optical volume, V_{eff}, is estimated to be *ca.* 60 zL (1 zL = 10^{-21} L), according to,

$$V_{eff} = \frac{\pi d^2 \Lambda}{24} \tag{1}$$

where the decay constant, Λ, defined as,[21, 47, 48]

$$\frac{1}{\Lambda} = 2\left[\left(\frac{1}{\lambda_c}\right)^2 - \left(\frac{1}{\lambda_m}\right)^2\right]^{1/2} \tag{2}$$

where λ_m is the wavelength in the ZMW medium. Thus, for the E-ZMW structures used here, single molecule average occupancy in the effective observation volume, *i.e.,* $\langle n \rangle = 1$, is achieved at a concentration of ~28 μM.

Electrochemical Characterization of MV-Mediated GR Reduction. First, the electrochemical response of GR was investigated on planar Au electrodes (*ca.* 0.28 cm^2). In the absence of MV, no cathodic faradaic current was observed in the cyclic voltammogram (CV) of GR and GSSG in the range –1.0 V ≤ E_{appl} ≤ –0.3 V, indicating negligible direct reduction of GR and GSSG at Au electrodes in this potential window, **Figure S2**. The redox-active centers, consisting of an FAD-binding domain proximal to a Cys-Cys disulfide bridge, are buried deep within the 118 kDa, ~120 × 62 × 84 Å GR structure,[49, 50] making direct electron transfer from the electrode surface inefficient. To overcome this issue, methyl viologen, MV^{2+}, was introduced as a redox mediator to shuttle electrons from the electrode to the GR active site(s), as depicted in **Figure**

2A.[42, 43] The electrochemical reduction of MV^{2+} to $MV^{+\bullet}$ is fast and electrochemically reversible on Au, and the reduction of GR_{ox} to GR_{red} is thermodynamically driven by $MV^{+\bullet}$, given the standard redox potentials of FAD/$FADH_2$ ($E^{\circ\prime}_{FAD} = -0.22$ V) and $MV^{2+}/MV^{+\bullet}$ ($E^{\circ} = -0.42$ V), **Figure 2B**. The voltammogram of 5 mM MV^{2+} in 0.1 M phosphate buffer (PB) and 0.1 M KNO_3 at pH 7.6 in **Figure 2C,** shows the cathodic $MV^{2+}/MV^{+\bullet}$ peak at *ca.* –0.87 V *vs.* Ag/AgCl. Notably, an additional current peak at *ca.* –0.65 V, is likely associated with $MV^{+\bullet}$-mediated oxygen reduction reaction,[51, 52] since the corresponding peak diminishes or disappears in solutions in which O_2 is rigorously excluded (data not shown).

Next, to confirm the $MV^{+\bullet}$-mediated reduction of GR, voltammetric responses were measured at increasing GR concentrations in the presence of 5 mM MV and 5 mM GSSG, **Figure 2D**. Cathodic current increases with increasing GR concentration, while oxidation peak current concurrently decreases, suggesting effective $MV^{+\bullet}$-mediated GR reduction. In other words, $MV^{+\bullet}$ acts as an electron donor, transferring electrons to GR, generating oxidized MV^{2+}, which is subsequently reduced electrochemically at the Au electrode, as depicted in **Figure 2A**, thus leading to the increasing cathodic current associated with MV^{2+} reduction. A plot of reaction rate as a function of GR concentration in **Figure S3** shows a linear response of enzymatic reaction rate to increasing enzyme concentration in the presence of a large excess of substrate.

The electrochemical response of the MV/GR/GSSG system was then investigated in E-ZMW nanopore arrays. Before commencing the main electrochemical experiments, the Au E-ZMW ring electrodes were cleaned by performing multiple CV scans in 0.5 M H_2SO_4 to remove residual damage and implantation from the ion milling process. The CVs in **Figure S4** show that both oxidation and reduction current responses are suppressed on the first cycle. However, the current gradually increases with increasing scan numbers and finally becomes much larger at the

19th cycle, reflecting facile oxidation of Au and subsequent reduction of the gold oxide formed, but not causing structural change, which was confirmed through SEM imaging.

Next, the voltammetric responses were obtained as a function of GSSG concentration in the presence of 5 mM MV and 6.5 μM GR in 0.1 M PB/0.1 M KNO_3 solution, **Figure 3**. In the presence of GR, the cathodic current due to MV^{2+} reduction increases with increasing GSSG concentration, **Figure 3A**. Since $MV^{+\bullet}$ does not directly react with GSSG (see **Figure S5D**), this observation implicates the enzymatic reduction of GSSG by GR. As shown in **Figure 2A**, GR_{red} is oxidized to GR_{ox} during the reduction of GSSG, and is subsequently reduced back to its initial state GR_{red} by $MV^{+\bullet}$, thus producing an increase in MV^{2+}, as reflected in the higher reduction peak current. The rate of enzyme reaction initially increases as substrate concentration increases, but once enzyme active sites become saturated, further increases in substrate concentration have negligible effect on the enzymatic reaction rate, resulting in the saturated current response observed at high concentration of GSSG in **Figure 3B**. Using a Michaelis-Menten model, as shown in **Figure S6**, we obtained the kinetic parameter for GR, *i.e.*, K_m value of *ca.* 83 μM, which is in reasonable agreement with the reported K_m value of 61 μM determined from large volume homogeneous assays.[53] Meanwhile, GSSG in the absence of GR, does not exhibit an increasing current response with concentration, with or without MV, as shown in **Figures S5D** and **S5C**, respectively. The slight current decrease with increasing GSSG concentration in **Figure S5C** is likely due to interaction between the Au surface and the disulfide GSSG, resulting in decreased accessible surface area. In contrast, addition of increasing amounts of GR to a solution with constant MV and GSSG, produces increasing cathodic MV currents, as shown in **Figure S7**, due to the catalytic activity of GR. Taken together these experiments illustrate that MV is an efficient redox mediator for the electron transfer between GR and Au and that the redox scheme shown in

Figure 2A accurately depicts the behavior in the presence of MV, GR, and GSSG.

Potential-Dependent GR Fluorescence in E-ZMWs. Having characterized the electrochemical behavior of MV/GR/GSSG in E-ZMWs, we next explored the *in situ* fluorescence behavior of GR under electrochemical potential control in E-ZMWs. Fluorescence measurements were performed on a wide-field epi-illumination microscope with illumination at 458 nm, and an EMCCD detector was used to detect the fluorescence emission, as shown schematically in **Figure 1A**. Typically, signals in a 5 pixel × 5 pixel region of interest (ROI), corresponding to 800 nm × 800 nm, were averaged to determine single-nanopore fluorescence intensities, as shown in **Figure 1B**. In the absence of applied potential, GR exhibits a low level of randomly-timed fluorescence emission events. Given that the 200 ms frame rate of the EMCCD camera is too slow to resolve individual fluorescence transitions, these emission events are interpreted to result from transport of individual GR molecules into/out of the nanopore being imaged. Furthermore, in the absence of MV, a potential-independent fluorescence response is observed upon the application of 10 s long potential steps between –0.95 V and 0.0 V *vs.* Ag/AgCl in 22 μM GR solution, where the average occupancy of the effective observation volume, $\langle n \rangle_{\text{eff}}$ is *ca.* 0.8, **Figure S8**. This is attributed to the inefficient electron transfer between the GR redox sites and the electrode, although GR is fluorescent in the oxidized state and non-fluorescent in the reduced state at 0.0 V and –0.95 V, respectively.

Fluorescence measurements were then conducted in the presence of 1 mM MV to examine the effectiveness of manipulating GR redox state by diffusing MV. The CV of 22 μM GR and 1 mM MV solution in **Figure 4A** displays cathodic and anodic peaks characteristic of MV in E-ZMWs at *ca*. –0.90 V and –0.84 V *vs*. Ag/AgCl, respectively, and thus the half-wave potential, $E_{1/2}$, is *ca*. –0.87 V. Because GR is effectively reduced only by MV-mediated electron transfer, the

fluorescence of freely-diffusing GR in nanopores was investigated by modulating the redox state of MV, and the fluorescence dynamics of GR were investigated by the application of multiple 10 s potential steps between –0.95 V and –0.75 V, as shown in **Figure 4B**. It is important to note that electrochemical signals shown in **Figure 4C** were collected by integrating over the entire array consisting of 3362 nanopores, whereas spectroscopic imaging permits interrogation of the fluorescence signals from individual nanopores containing a single (or a few) molecule(s) at relatively high signal-to-noise ratio. As shown in **Figures 4D and S9**, the fluorescence signals from single nanopores containing both GR and MV, respond to the external potentials by exhibiting higher fluorescence intensities at oxidizing potentials, which is obvious upon from the averaged fluorescence response from 350 pores shown in **Figure 4F**, the side-by-side image comparison of the E-ZMW arrays at –0.95 V and –0.75 V in **Figure 4G**, and the application of Savitzky-Golay smoothing to single pore fluorescence data in **Figure S9**. Importantly, the potential dependence of the fluorescence recorded from nanopores containing MV-only solution in the absence of GR is insignificant, as shown in **Figure S10D**, verifying that the dynamic fluorescence changes are caused by redox state changes of GR.

Clearly, the distinct fluorescence behavior obtained upon the application of different external potentials in E-ZMWs results from the manipulation of the GR redox state by MV-mediated electron transfer. At the more negative potential, E_{appl} = –0.95 V, MV^{2+} is reduced to $MV^{+\bullet}$ which then donates electrons to one of the FAD cofactors in GR_{ox}, reducing it to $FADH_2$ in a $2e^-/2H^+$ process, resulting in lower fluorescence signals. On the other hand, when E_{appl} = –0.75 V, MV^{2+} is the dominant redox state, and MV-mediated GR reduction is negated. Reduced GR can subsequently either be reoxidized by an available oxidant, *e.g.* adventitious O_2 or a specific oxidant, such as GSSG, or it can diffuse out and be replaced by a new GR molecule diffusing into the

nanopore. As an additional check on this interpretation, the fluorescence response was monitored by applying either a reducing or an oxidizing potential in the middle of a time window for which the potential was otherwise held at open circuit potential, **Figure S11**. As expected, at –0.95 V, the fluorescence intensity decreases consistent with MV-mediated GR reduction resulting in a non-fluorescent GR in the observation volume. However, once the electrode is returned to OCP (**Figure S11**(*left*)), the fluorescence signal increases, even though no external potential is applied, consistent with repopulation of the nanopore by oxidized GR, which is the dominant form present in bulk solution. On the other hand, when E_{appl} = 0.0 V is applied in the middle of an OCP window, the fluorescence intensity remains unchanged. Finally we note there is significant pore-to-pore heterogeneity in fluorescence intensity levels at either oxidizing or reducing potentials, as shown by the single molecule fluorescence images in **Figure 4G**. These pore-to-pore differences in fluorescence reflect differences in (*a*) average pore occupation (predominantly $\langle n \rangle$ = 0 or 1) during the time window over which signals are integrated, (*b*) axial position of the fluorescent GR molecule relative to the evanescent field, and (*c*) the presence and proximity of any quenching agents.

Fluorescence Response to GSSG. Finally, the fluorescence dynamics of GR was monitored in response to the presence and concentration of the enzyme substrate, *i.e.,* GSSG, by comparing fluorescence signals obtained in the absence and presence of GSSG in 22 μM GR and 1 mM MV solution in E-ZMWs, **Figure 5**. Multiple potential steps between –0.95 V and –0.75 V were applied to the Au ring electrodes, and fluorescence signals from nanopores were recorded for 60 s. When E_{appl} is set to a reducing value, –0.95 V, very little difference in the fluorescence histograms is observed upon the addition of GSSG, **Figure 5A**. However, when the potential is set to a more oxidizing value, –0.75 V, a readily apparent change in fluorescence histograms is observed in

response to GSSG addition, **Figure 5B**. These observations are consistent with a picture in which GR is continuously reduced by $MV^{+\bullet}$ at –0.95 V, even in the presence of relatively high concentrations, 5 mM, of enzyme substrate, suggesting that GR_{ox} is effectively reduced by $MV^{+\bullet}$ before it can substantially affect the fluorescence intensity. However, when the potential is switched to the more oxidizing –0.75 V, there is insufficient reduced $MV^{+\bullet}$ to effectively reduce the GSSG-oxidized GR, thereby resulting in higher fluorescence intensities with increasing GSSG concentration. Clearly, after the application of a reducing potential step (–0.95 V) both GR_{ox} and GR_{red} are present in solution. Then, the addition of GSSG shown in **Figure 5B** results in an increase in fluorescence, because GSSG promotes the reoxidation of the GR_{red} produced from the previous potential step. This behavior is confirmed by comparing the histograms obtained with E_{appl} = –0.95 V and –0.75 V in the presence of 1 mM GSSG, **Figure 5C**. These data clearly show that a meaningful response is obtained in the presence of GSSG upon switching the potential from –0.95 V to –0.75 V, consistent with the fluorescence from GR_{ox} being determined by the interplay between $MV^{2+/+\bullet}$ and GSSG/GSH, as discussed above and shown in **Figure 2A**.

Conclusions

In this work, freely-diffusing single GR enzyme molecules are interrogated in single Au ring electrode-embedded E-ZMWs, where the optical radiation is confined within a sub-volume of the nanopores, generating observation volumes of *ca.* 60 zL. This observation volume yields average occupancy of $\langle n \rangle = 0.8$ GR molecules per pore at 22 μM bulk GR concentration, thereby supporting single molecule studies in the E-ZMWs. In addition, the ZMW metal cladding layer does double duty, also functioning as a working electrode, which is embedded in the nanopore array, enabling real-time spectroelectrochemical cross-correlation studies of single redox-active

enzyme molecules. Since direct electron transfer to/from the working electrode to the active redox sites of GR is challenging, a mediated electron transfer strategy was adopted employing MV as the mediator. MV is an efficient mediator for GR redox, as demonstrated by both electrochemical and fluorescence characterization of MV/GR/GSSG-containing E-ZMW nanopore arrays. Specific evidence for this interpretation includes: (1) increasing cathodic current in response to GR-mediated oxidation of $MV^{+\bullet}$ producing MV^{2+}, (2) lower fluorescence intensities from GR observed when the Au ring electrodes are held at reducing potentials and higher intensities at oxidizing potentials, and (3) increasing fluorescence in response to increasing concentrations of the enzyme substrate, GSSG, as well as higher cathodic currents (from MV^{2+} reduction).

E-ZMWs represent a promising platform for *in situ* spectroelectrochemical investigations of single enzyme molecules, since they make it possible to address small probe volumes under tightly-controlled conditions, allowing high-throughput simultaneous detection from massively parallel arrays of nanopores. Clearly, because the current studies utilized freely diffusing enzymes at single occupancy concentrations, signals were necessarily integrated over many individual molecules during the acquisition period of the camera. Next, we will immobilize enzymes on the nanopore electrode surface with special attention to controlling enzyme orientation, so that the fluorescence-correlated electrochemistry approach developed in this study can be applied to quantify the fluorescence signals of GR_{ox}/GR_{red} conversion, enzyme turnover, heterogeneity of subpopulations, and response of enzymes to environmental stresses, *e.g.,* reactive oxygen species (ROS), generated *in situ* in nanopores. Thus, E-ZMWs not only enable effective experimental strategies for single molecule enzyme studies, but also represent a platform capable of providing insights for disease-targeted research, such as the ROS-related diseases.

Associated content

Supporting Information: The Supporting Information is available free of charge on the ACS Publications website

Fabrication of E-ZMW devices; electrochemical characterization of E-ZMW solution components; electrochemical cleaning of Au surface; spectroelectrochemical response of GR-only and MV-only solutions; fluorescence response of GR+MV solution in between OCP and reducing (or oxidizing) potential

Author information

Corresponding Author

*E-mail: pbohn@nd.edu. Tel.: +1 574 631 1849. Fax: +1 574 631 8366.

ORCID

Seol Baek: 0000-0003-2191-6723

Donghoon Han: 0000-0003-1870-3006

Seung-Ryong Kwon: 0000-0002-0890-523X

Vignesh Sundaresan: 0000-0001-9390-1681

Paul W. Bohn: 0000-0001-9052-0349

Notes

The authors declare no competing financial interest.

Acknowledgements

This work was supported by the National Institute for General Medical Science through

grant 1R21GM126246-01 and the National Science Foundation through grant CHE1904196. We gratefully acknowledge the Notre Dame Nanofabrication Facility and the Notre Dame Integrated Imaging Facility, for their expert assistance in device fabrication and characterization.

References

1. Claessen, V. I.; Engelkamp, H.; Christianen, P. C. M.; Maan, J. C.; Nolte, R. J. M.; Blank, K.; Rowan, A. E. Single-Biomolecule Kinetics: The Art of Studying a Single Enzyme. *Annu. Rev. Anal. Chem.* **2010,** *3*, 319-340.

2. English, B. P.; Min, W.; van Oijen, A. M.; Lee, K. T.; Luo, G.; Sun, H.; Cherayil, B. J.; Kou, S. C.; Xie, X. S. Ever-Fluctuating Single Enzyme Molecules: Michaelis-Menten Equation Revisited. *Nat. Chem. Biol.* **2006,** *2*, 87-94.

3. Min, W.; English, B. P.; Luo, G.; Cherayil, B. J.; Kou, S. C.; Xie, X. S. Fluctuating Enzymes: Lessons from Single-Molecule Studies. *Acc. Chem. Res.* **2005,** *38*, 923-931.

4. Smiley, R. D.; Hammes, G. G. Single Molecule Studies of Enzyme Mechanisms. *Chem. Rev.* **2006,** *106*, 3080-3094.

5. Hatzakis, N. S. Single Molecule Insights on Conformational Selection and Induced Fit Mechanism. *Biophys. Chem.* **2014,** *186*, 46-54.

6. Xie, X. S.; Lu, H. P. Single-Molecule Enzymology*. *J. Biol. Chem.* **1999,** *274*, 15967-15970.

7. Chen, Q.; Groote, R.; Schönherr, H.; Vancso, G. J. Probing Single Enzyme Kinetics in Real-Time. *Chem. Soc. Rev.* **2009,** *38*, 2671-2683.

8. Laursen, T.; Singha, A.; Rantzau, N.; Tutkus, M.; Borch, J.; Hedegård, P.; Stamou, D.; Møller, B. L.; Hatzakis, N. S. Single Molecule Activity Measurements of Cytochrome P450 Oxidoreductase Reveal the Existence of Two Discrete Functional States. *ACS Chem. Biol.* **2014,** *9*, 630-634.

9. Brown, J. W. P.; Bauer, A.; Polinkovsky, M. E.; Bhumkar, A.; Hunter, D. J. B.; Gaus, K.; Sierecki, E.; Gambin, Y. Single-Molecule Detection on a Portable 3D-Printed Microscope. *Nature*

Communications **2019,** *10*, 5662.

10. Lu, S.-M.; Peng, Y.-Y.; Ying, Y.-L.; Long, Y.-T. Electrochemical Sensing at a Confined Space. *Anal. Chem.* **2020,** *92*, 5621-5644.

11. Fu, K.; Kwon, S.-R.; Han, D.; Bohn, P. W. Single Entity Electrochemistry in Nanopore Electrode Arrays: Ion Transport Meets Electron Transfer in Confined Geometries. *Acc. Chem. Res.* **2020,** *53*, 719-728.

12. Baker, L. A. Perspective and Prospectus on Single-Entity Electrochemistry. *J. Am. Chem. Soc.* **2018,** *140*, 15549-15559.

13. Lemay, S. G.; Kang, S.; Mathwig, K.; Singh, P. S. Single-Molecule Electrochemistry: Present Status and Outlook. *Acc. Chem. Res.* **2013,** *46*, 369-377.

14. Fan, F.-R. F.; Bard, A. J. Electrochemical Detection of Single Molecules. *Science* **1995,** *267*, 871-874.

15. Fan, Y.; Anderson, T. J.; Zhang, B. Single-Molecule Electrochemistry: From Redox Cycling to Single Redox Events. *Curr. Opin. Electrochem.* **2018,** *7*, 81-86.

16. Sun, P.; Mirkin, M. V. Electrochemistry of Individual Molecules in Zeptoliter Volumes. *J. Am. Chem. Soc.* **2008,** *130*, 8241-8250.

17. Chen, Q.; McKelvey, K.; Edwards, M. A.; White, H. S. Redox Cycling in Nanogap Electrochemical Cells. The Role of Electrostatics in Determining the Cell Response. *J. Phys. Chem. C* **2016,** *120*, 17251-17260.

18. Palacios, R. E.; Fan, F.-R. F.; Bard, A. J.; Barbara, P. F. Single-Molecule Spectroelectrochemistry (SMS-EC). *J. Am. Chem. Soc.* **2006,** *128*, 9028-9029.

19. Lu, J.; Fan, Y.; Howard, M. D.; Vaughan, J. C.; Zhang, B. Single-Molecule Electrochemistry on a Porous Silica-Coated Electrode. *J. Am. Chem. Soc.* **2017,** *139*, 2964-2971.

20. Moerner, W. E.; Fromm, D. P. Methods of Single-Molecule Fluorescence Spectroscopy and Microscopy. *Rev. Sci. Instrum.* **2003,** *74*, 3597-3619.

21. Crouch, G. M.; Han, D.; Bohn, P. W. Zero-Mode Waveguide Nanophotonic Structures for Single Molecule Characterization. *J. Phys. D: Appl. Phys.* **2018,** *51*, 193001.

22. Levene, M. J.; Korlach, J.; Turner, S. W.; Foquet, M.; Craighead, H. G.; Webb, W. W. Zero-Mode Waveguides for Single-Molecule Analysis at High Concentrations. *Science* **2003,** *299*, 682-686.

23. Zhao, J.; Zaino Iii, L. P.; Bohn, P. W. Potential-Dependent Single Molecule Blinking Dynamics for Flavin Adenine Dinucleotide Covalently Immobilized in Zero-Mode Waveguide Array of Working Electrodes. *Faraday Discuss.* **2013,** *164*, 57-69.

24. Zhu, P.; Craighead, H. G. Zero-Mode Waveguides for Single-Molecule Analysis. *Annu. Rev. Biophys.* **2012,** *41*, 269-293.

25. Richards, C. I.; Luong, K.; Srinivasan, R.; Turner, S. W.; Dougherty, D. A.; Korlach, J.; Lester, H. A. Live-Cell Imaging of Single Receptor Composition Using Zero-Mode Waveguide Nanostructures. *Nano Lett.* **2012,** *12*, 3690-3694.

26. Jadhav, V.; Hoogerheide, D. P.; Korlach, J.; Wanunu, M. Porous Zero-Mode Waveguides for Picogram-Level DNA Capture. *Nano Lett.* **2019,** *19*, 921-929.

27. Larkin, J.; Henley, R. Y.; Jadhav, V.; Korlach, J.; Wanunu, M. Length-Independent DNA Packing into Nanopore Zero-Mode Waveguides for Low-Input DNA Sequencing. *Nat. Nanotechnol.* **2017,** *12*, 1169-1175.

28. Eid, J.*, et al.* Real-Time DNA Sequencing from Single Polymerase Molecules. *Science* **2009,** *323*, 133-138.

29. Uemura, S.; Aitken, C. E.; Korlach, J.; Flusberg, B. A.; Turner, S. W.; Puglisi, J. D. Real-

Time tRNA Transit on Single Translating Ribosomes at Codon Resolution. *Nature* **2010,** *464*, 1012-1017.

30. Vilfan, I. D.; Tsai, Y.-C.; Clark, T. A.; Wegener, J.; Dai, Q.; Yi, C.; Pan, T.; Turner, S. W.; Korlach, J. Analysis of RNA Base Modification and Structural Rearrangement by Single-Molecule Real-Time Detection of Reverse Transcription. *J. Nanobiotechnol.* **2013,** *11*, 8.

31. Zhao, J.; Branagan, S. P.; Bohn, P. W. Single-Molecule Enzyme Dynamics of Monomeric Sarcosine Oxidase in a Gold-Based Zero-Mode Waveguide. *Appl. Spectrosc.* **2012,** *66*, 163-169.

32. Miyake, T.; Tanii, T.; Sonobe, H.; Akahori, R.; Shimamoto, N.; Ueno, T.; Funatsu, T.; Ohdomari, I. Real-Time Imaging of Single-Molecule Fluorescence with a Zero-Mode Waveguide for the Analysis of Protein−Protein Interaction. *Anal. Chem.* **2008,** *80*, 6018-6022.

33. Sandén, T.; Wyss, R.; Santschi, C.; Hassaïne, G.; Deluz, C.; Martin, O. J. F.; Wennmalm, S.; Vogel, H. A Zeptoliter Volume Meter for Analysis of Single Protein Molecules. *Nano Lett.* **2012,** *12*, 370-375.

34. Goldschen-Ohm, M. P.; Klenchin, V. A.; White, D. S.; Cowgill, J. B.; Cui, Q.; Goldsmith, R. H.; Chanda, B. Structure and Dynamics Underlying Elementary Ligand Binding Events in Human Pacemaking Channels. *ELife* **2016,** *5: e20797*.

35. Han, D.; Crouch, Garrison M.; Fu, K.; Zaino Iii, L. P.; Bohn, P. W. Single-Molecule Spectroelectrochemical Cross-Correlation During Redox Cycling in Recessed Dual Ring Electrode Zero-Mode Waveguides. *Chem. Sci.* **2017,** *8*, 5345-5355.

36. Mannervik, B. The Enzymes of Glutathione Metabolism: an Overview. *Biochem. Soc. Trans.* **1987,** *15*, 717-718.

37. Espinosa-Diez, C.; Miguel, V.; Mennerich, D.; Kietzmann, T.; Sánchez-Pérez, P.; Cadenas, S.; Lamas, S. Antioxidant Responses and Cellular Adjustments to Oxidative Stress. *Redox Biol*

2015, *6*, 183-197.

38. Lu, H. P.; Xun, L.; Xie, X. S. Single-Molecule Enzymatic Dynamics. *Science* **1998,** *282*, 1877-1882.

39. Berndt, N.; Kovács, R.; Rösner, J.; Wallach, I.; Dreier, J. P.; Liotta, A. Flavin Adenine Dinucleotide Fluorescence as an Early Marker of Mitochondrial Impairment During Brain Hypoxia. *Int. J. Mol. Sci.* **2020,** *21*, 3977.

40. Krauth-Siegel, R. L.; Arscott, L. D.; Schönleben-Janas, A.; Schirmer, R. H.; Williams, C. H. Role of Active Site Tyrosine Residues in Catalysis by Human Glutathione Reductase. *Biochemistry* **1998,** *37*, 13968-13977.

41. van den Berg, P. A.; van Hoek, A.; Walentas, C. D.; Perham, R. N.; Visser, A. J. Flavin Fluorescence Dynamics and Photoinduced Electron Transfer in Escherichia Coli Glutathione Reductase. *Biophys J* **1998,** *74*, 2046-2058.

42. Willner, I.; Katz, E.; Riklin, A.; Kasher, R. Mediated electron transfer in gluthathione reductase organized in self-assembled monolayers on gold electrodes. *J. Am. Chem. Soc.* **1992,** *114*, 10965-10966.

43. Willner, I.; Lapidot, N.; Riklin, A.; Kasher, R.; Zahavy, E.; Katz, E. Electron-Transfer Communication in Glutathione Reductase Assemblies: Electrocatalytic, Photocatalytic, and Catalytic Systems for the Reduction of Oxidized Glutathione. *J. Am. Chem. Soc.* **1994,** *116*, 1428-1441.

44. Bollella, P.; Katz, E. Enzyme-Based Biosensors: Tackling Electron Transfer Issues. *Sensors (Basel)* **2020,** *20*, 3517.

45. Carano, M.; Cosnier, S.; Kordatos, K.; Marcaccio, M.; Margotti, M.; Paolucci, F.; Prato, M.; Roffia, S. A Glutathione Amperometric Biosensor Based on an Amphiphilic Fullerene Redox

Mediator Immobilised Within an Amphiphilic Polypyrrole Film. *J. Mater. Chem.* **2002,** *12*, 1996-2000.

46. Han, D.; Zaino, L. P.; Fu, K.; Bohn, P. W. Redox Cycling in Nanopore-Confined Recessed Dual-Ring Electrode Arrays. *J. Phys. Chem. C* **2016,** *120*, 20634-20641.

47. Zaino, L. P.; Grismer, D. A.; Han, D.; Crouch, G. M.; Bohn, P. W. Single Occupancy Spectroelectrochemistry of Freely Diffusing Flavin Mononucleotide in Zero-Dimensional Nanophotonic Structures. *Faraday Discuss.* **2015,** *184*, 101-115.

48. Moran-Mirabal, J. M.; Craighead, H. G. Zero-Mode Waveguides: Sub-Wavelength Nanostructures for Single Molecule Studies at High Concentrations. *Methods* **2008,** *46*, 11-17.

49. Pai, E. F.; Schulz, G. E. The Catalytic Mechanism of Glutathione Reductase as Derived from X-Ray Diffraction Analyses of Reaction Intermediates. *J Biol Chem* **1983,** *258*, 1752-1757.

50. Berkholz, D. S.; Faber, H. R.; Savvides, S. N.; Karplus, P. A. Catalytic Cycle of Human Glutathione Reductase Near 1 A Resolution. *J Mol Biol* **2008,** *382*, 371-384.

51. Bennett, T.; Niroomand, H.; Pamu, R.; Ivanov, I.; Mukherjee, D.; Khomami, B. Elucidating the Role of Methyl Viologen as a Scavenger of Photoactivated Electrons from Photosystem I Under Aerobic and Anaerobic Conditions. *Phys. Chem. Chem. Phys.* **2016,** *18*, 8512-8521.

52. Lin, Q.; Li, Q.; Batchelor-McAuley, C.; Compton, R. G. Use of 'Split Waves' for the Measurement of Electrocatalytic Kinetics: Methyl Viologen Mediated Oxygen Reduction on a Boron-Doped Diamond Electrode. *Phys. Chem. Chem. Phys.* **2013,** *15*, 7760-7767.

53. Mavis, R. D.; Stellwagen, E. Purification and Subunit Structure of Glutathione Reductase from Bakers' Yeast. *J. Biol. Chem.* **1968,** *243*, 809-814.

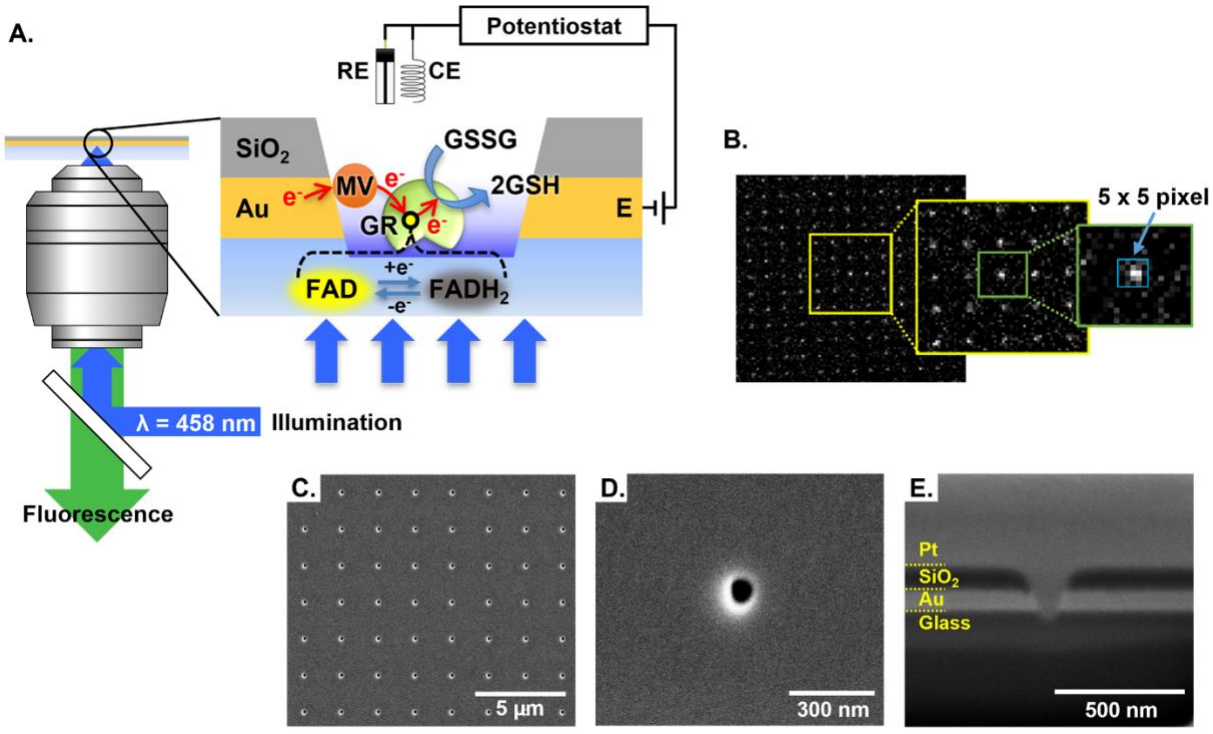

Figure 1. **A.** Schematic illustration of the E-ZMW device to monitor spectroelectrochemistry of freely-diffusing GR molecules v*ia* epi-illumination wide-field fluorescence microscopy. Electrochemical potential at the Au ring electrode is controlled using a potentiostat in a 3-electrode configuration with Pt wire and Ag/AgCl counter and reference electrodes, respectively, placed outside the nanopores. **B**. Magnified fluorescence images of E-ZMW array containing GR. Typically, a 5 × 5 pixel-area was selected to locate a single nanopore, *i.e.,* region of interest (ROI), and mean fluorescence signals were obtained by averaging the signals over the ROI. **C-D**. Top-view SEM images of a subsection of the nanopore array (**C**) and a single nanopore (**D**). **E.** Cross-sectional SEM image of a single ring electrode embedded in a nanopore.

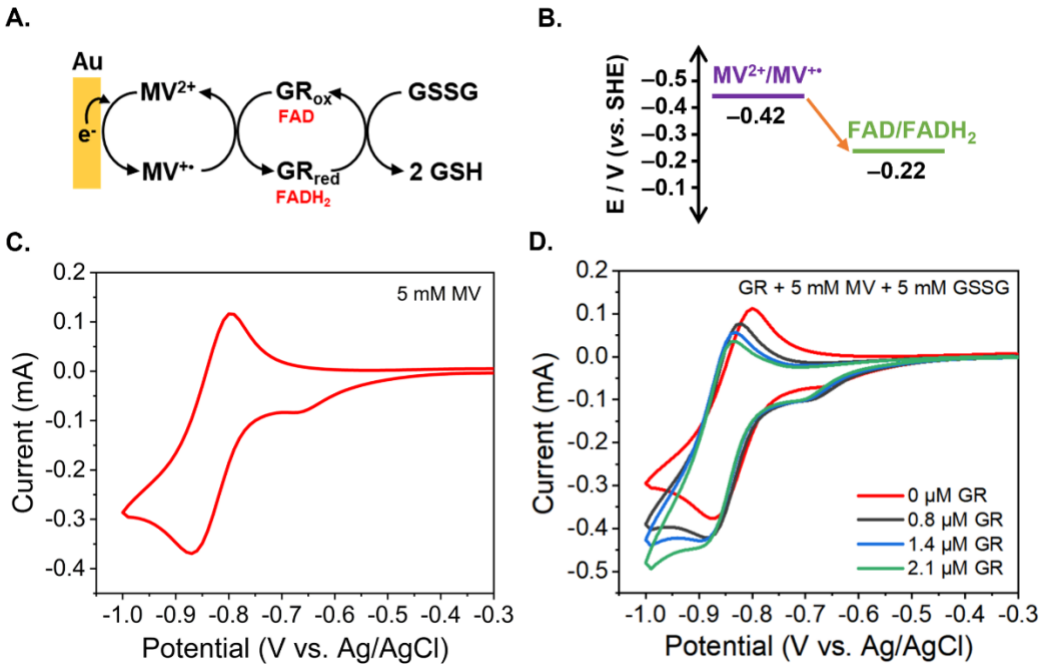

Figure 2. **A.** Cascade electron transfer reactions involved in MV-mediated GR enzymatic reactions in the presence of GSSG on Au. **B.** Standard reduction potentials of $MV^{2+}/MV^{+\bullet}$ and $FAD/FADH_2$. **C-D**. CVs of 5 mM MV (C), and 5 mM MV + 5 mM GSSG with different concentrations of GR (D) in 0.1 M PB/0.1 M KNO_3 at pH 7.6, on planar Au (A ~ 0.28 cm^2). Scan rate: 100 mV s^{-1}.

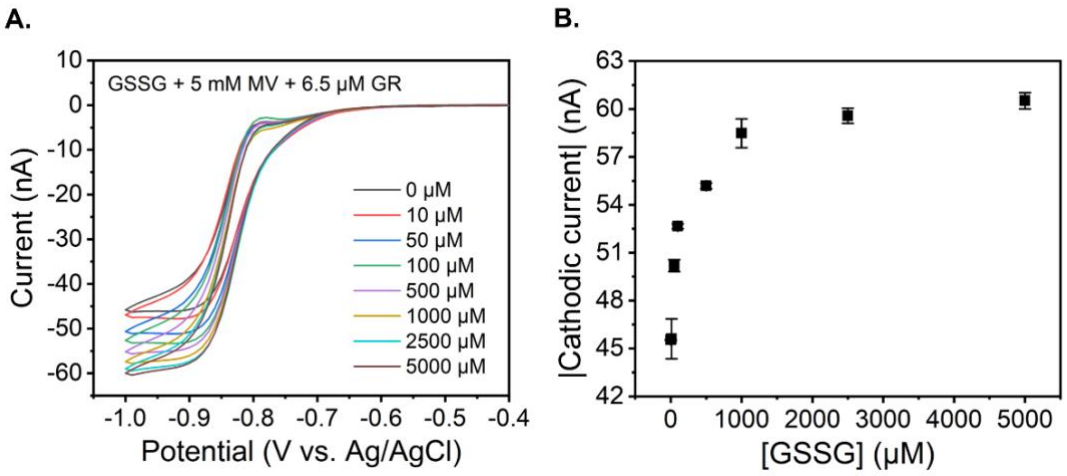

Figure 3. **A.** CVs of 5 mM MV + 6.5 µM GR in 0.1 M PB and 0.1M KNO_3 solution (pH 7.6) as a function of GSSG concentration, obtained in an E-ZMW array. **B**. Plot of cathodic current as a function of GSSG concentration. Current values were taken from the cathodic current at –1.0 V in panel **A**. Error bars represent the standard deviation (n = 3). Scan rate: 50 mV s^{-1}.

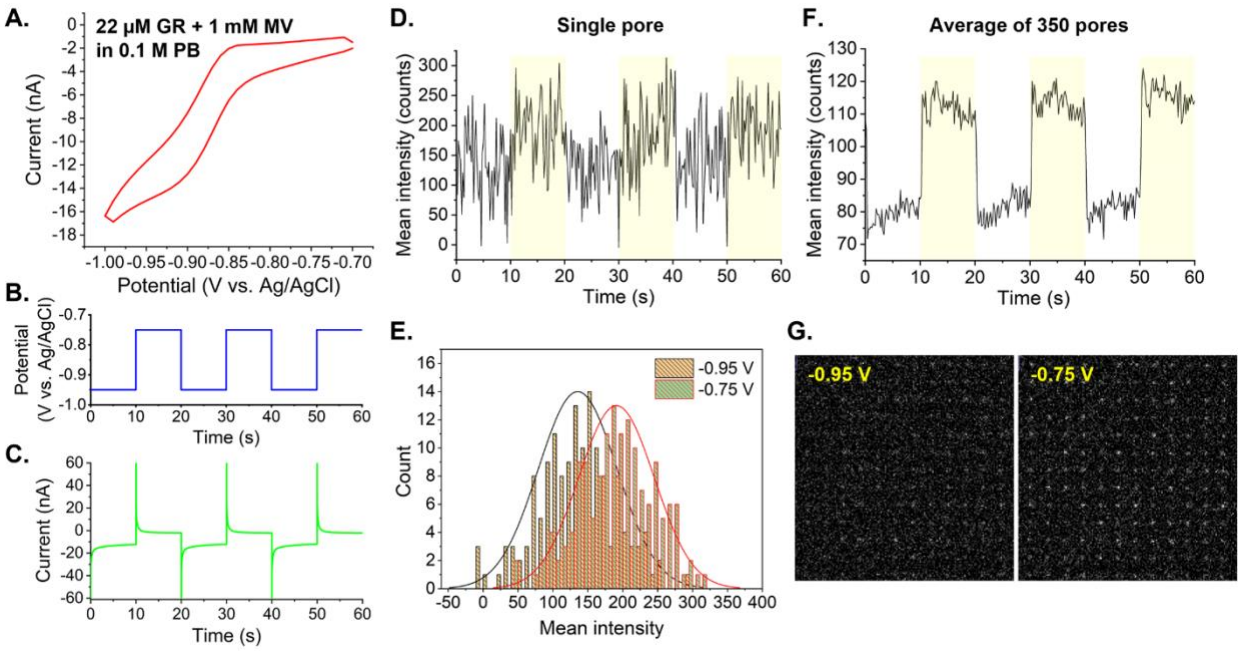

Figure 4. Spectroelectrochemical response to the potential perturbation in E-ZMWs containing 22 μM GR and 1 mM MV in 0.1 M PB at pH 7.6. Under these conditions the average pore occupancy $\langle n \rangle_{\text{eff}} \sim 0.8$ **A.** Voltammetric response of GR and MV in 0.1 M PB, **B**. Multiple potential step modulation between –0.95 V and –0.75 V at 10 s intervals for 60 s. **C**. Current response to multi-potential steps from 22 μM GR and 1 mM MV. **D**. Background-subtracted fluorescence signals from a representative single pore. **E**. Distribution of mean fluorescence intensities from single pores at the applied potential steps, as shown in panel **D**. **F**. Background-subtracted average fluorescence signals from 350 pores. **G**. Fluorescence frame images obtained at –0.95 V and –0.75 V. Acquisition time for fluorescence signals is 200 ms/frame.

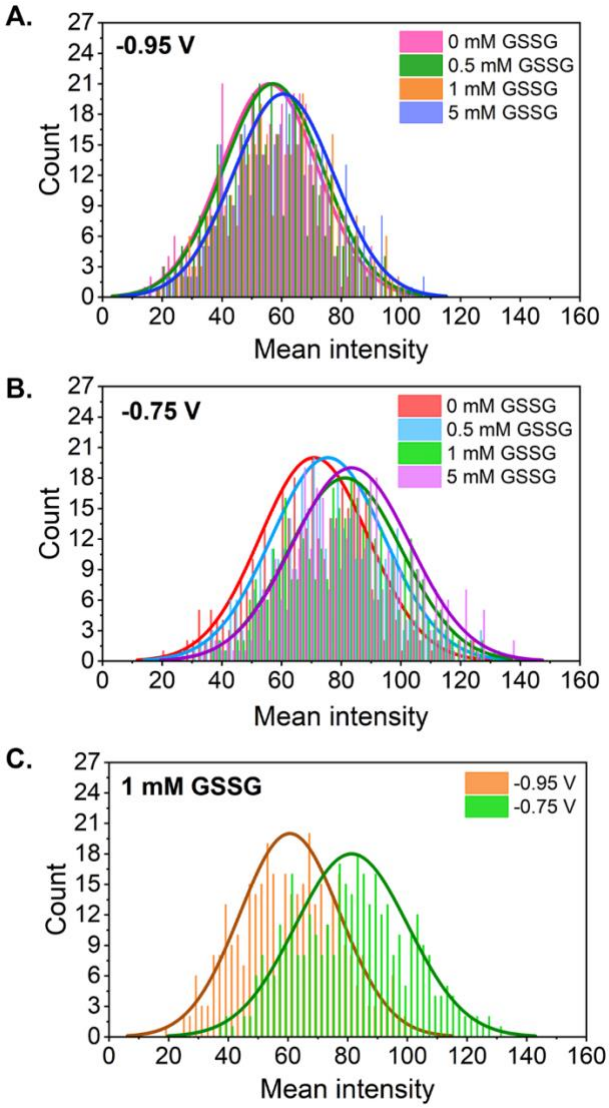

Figure 5. A-B. Distribution of average single pore fluorescence signals from E-ZMW pores containing 22 μM GR ($\langle n \rangle_{eff} \sim 0.8$), 1 mM MV and different concentrations of GSSG in 0.1 M PB at pH 7.6. The electrode potential was set to –0.95 V (**A**) or –0.75 V (**B**). **C**. Fluorescence response distribution of 1 mM GSSG in 22 μM GR and 1 mM MV solution at –0.95 V and –0.75 V. In all panels, histograms represent individual intensity bins, and solid lines are fits to Gaussian distributions.

TOC graphic

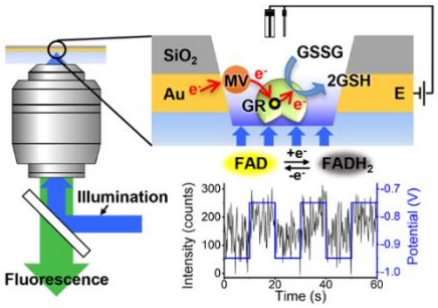
SiO2
Au
MV
GR
GSSG
2GSH
E
FAD
FADH2
Illumination
Fluorescence
Intensity (counts)
Potential (V)
Time (s)

Supporting Information for

Electrochemical Zero-Mode Waveguide Potential-Dependent Fluorescence of Glutathione Reductase at Single-Molecule Occupancy

Seol Baek[1], Donghoon Han[2], Seung-Ryong Kwon[3], Vignesh Sundaresan[4], and Paul W. Bohn[1,4*]

[1]Department of Chemistry and Biochemistry, University of Notre Dame, Notre Dame, Indiana 46556, United States

[2]Department of Chemistry, The Catholic University of Korea, Bucheon, Gyeonggi-do 14662, South Korea

[3]Department of Chemistry and Research Institute of Natural Science, Gyeongsang National University, Jinju, 52828, South Korea

[4]Department of Chemical and Biomolecular Engineering, University of Notre Dame, Notre Dame, Indiana 46556, United States

[*]Author to whom correspondence should be addressed, *pbohn@nd.edu*

Table of Contents

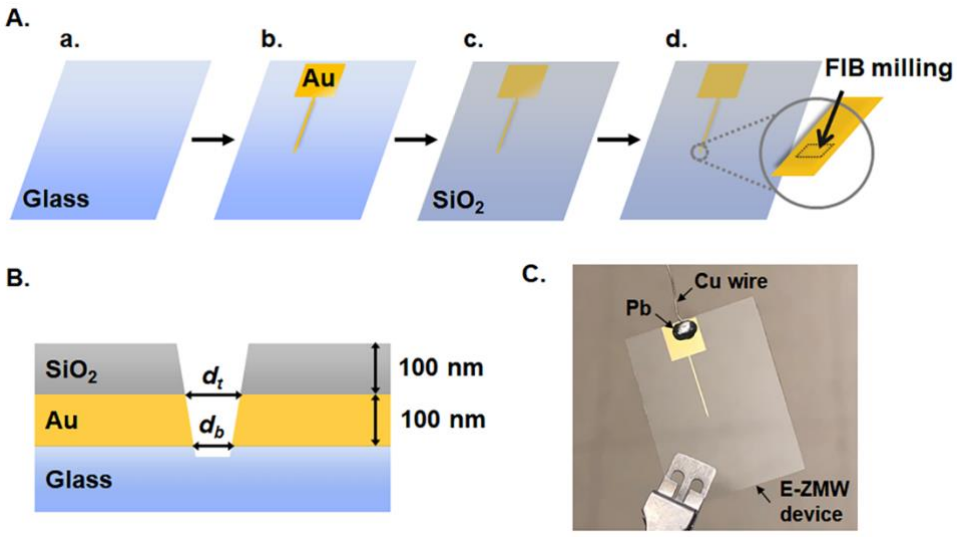

Figure S1. **A**. Schematic illustration showing the fabrication procedure for E-ZMW devices. **a**. Pre-cleaned glass slide, **b**. photolithography and Au deposition, **c**. SiO_2 deposition, **d**. FIB milling. **B**. Schematic cross-sectional diagram of a single ring electrode embedded in a nanopore with a top diameter, d_t ~ 110 nm, and a bottom diameter, d_b ~ 80 nm. **C**. Optical image of a typical E-ZMW device.

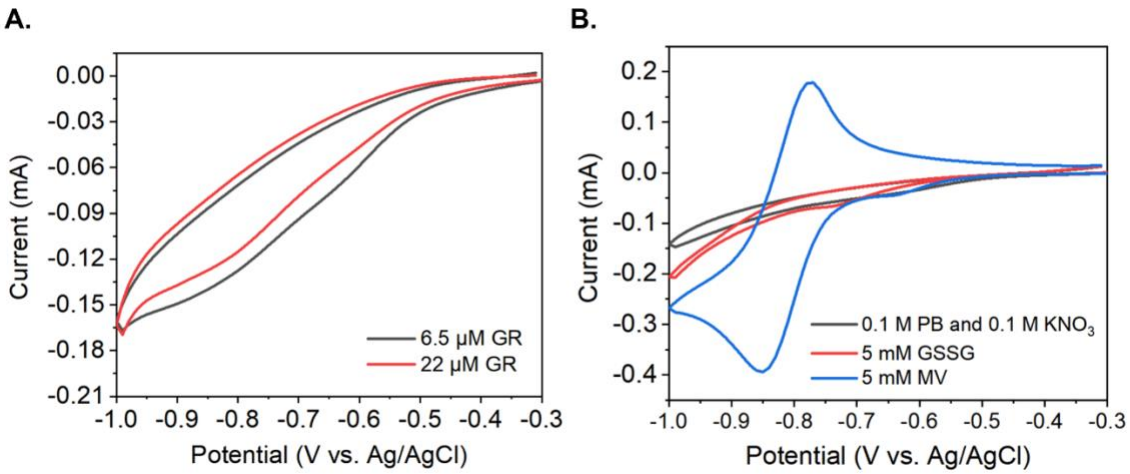

Figure S2. Cyclic voltammetry E-ZMW solution components. **A.** GR at 6.5 µM (gray) and 22 µM (red). **B**. supporting electrolyte plus buffer (gray), 5 mM GSSG (red), and 5 mM MV in 0.1 M PB and 0.1 M KNO_3 at pH 7.6 (blue).

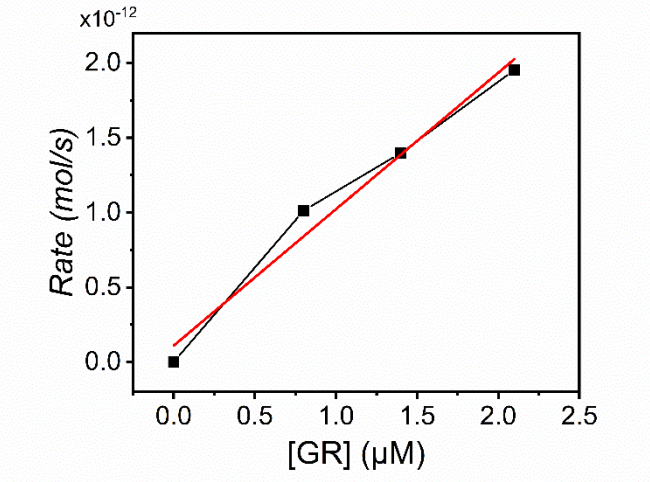

Figure S3. Plot of reaction rate as a function of GR concentration. Each data point was obtained from the increase in the cathodic current at −1.0 V in comparison with the current at [GR] = 0 µM in **Figure 2D**. The red line represents a linear fit for the plot (R^2 = 0.98).

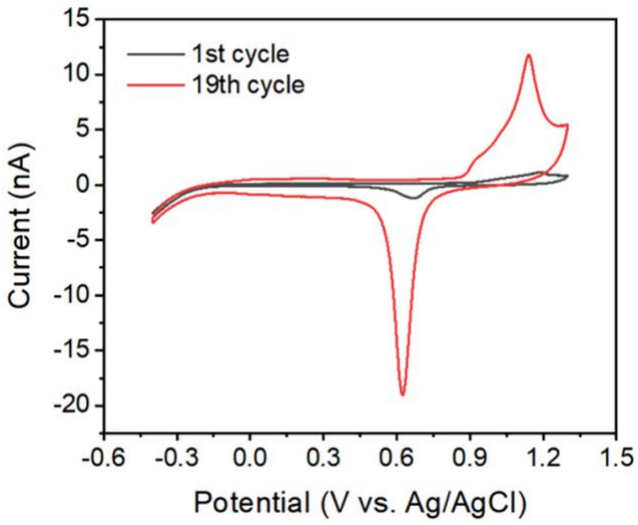

Figure S4. Successive cyclic voltammograms (CVs) of Au electrode in nanopore arrays containing 0.5 M H_2SO_4 for electrochemical cleaning. CVs at 1st (gray) and 19th (red) cycle are depicted.

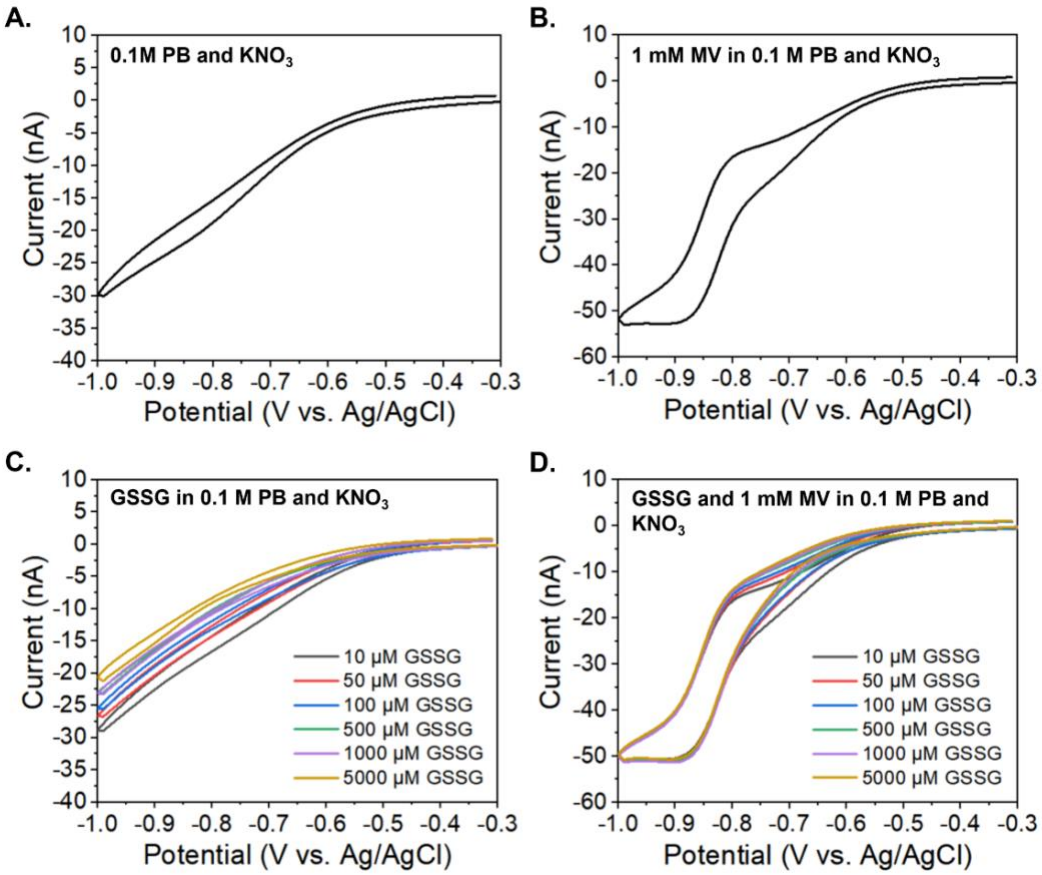

Figure S5. Cyclic voltammetry control experiments. **A**. Supporting electrolyte 0.1 M PB/0.1 M KNO_3. **B**. 1 mM MV in supporting electrolyte. **C**. GSSG at various concentrations in supporting electrolyte. **D**. GSSG at various concentrations and 1 mM MV in supporting electrolyte. All data were acquired from E-ZMW nanopore arrays.

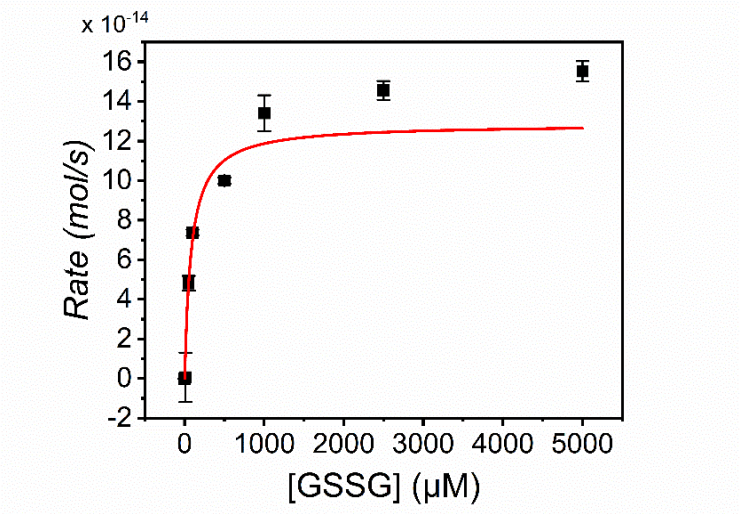

Figure S6. Plot of reaction rate as a function of GSSG concentration. Each data point represents the increase value of the cathodic current at −1.0 V in comparison with the current at [GSSG] = 0 μM in **Figure 3A**. The red line is a fit to Michaelis-Menten kinetics.

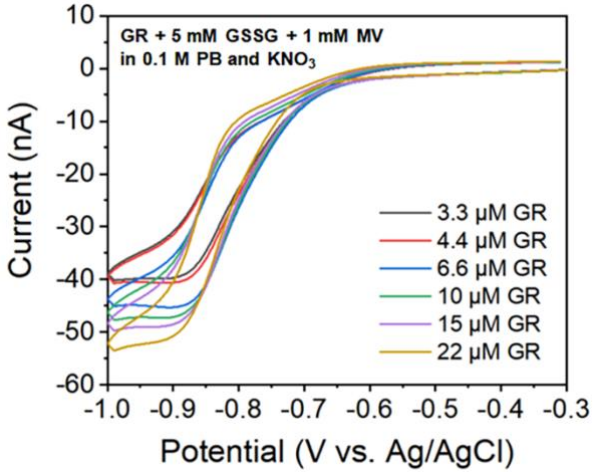

Figure S7. Voltammetric response from GR addition into 1 mM MV and 5 mM GSSG in 0.1 M PB and 0.1 M KNO_3 at pH 7.6 in nanopore arrays.

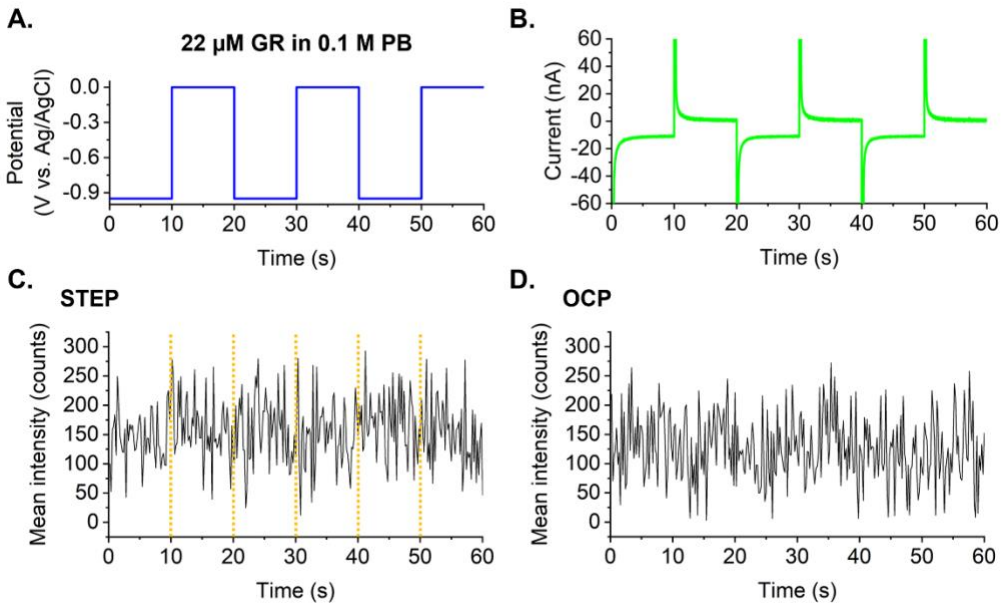

Figure S8. Spectroelectrochemical response of 22 µM GR in 0.1 M PB in E-ZMWs, conditions where the average pore occupancy $\langle n \rangle_{\text{eff}} \sim 0.8$. **A**. Step potential-time plot. **B**. Current response. **C**. Representative fluorescence trajectory from a single pore under step-potential program in panel (**A**). **D**. Representative fluorescence trajectory at open circuit potential (OCP) obtained from a single pore.

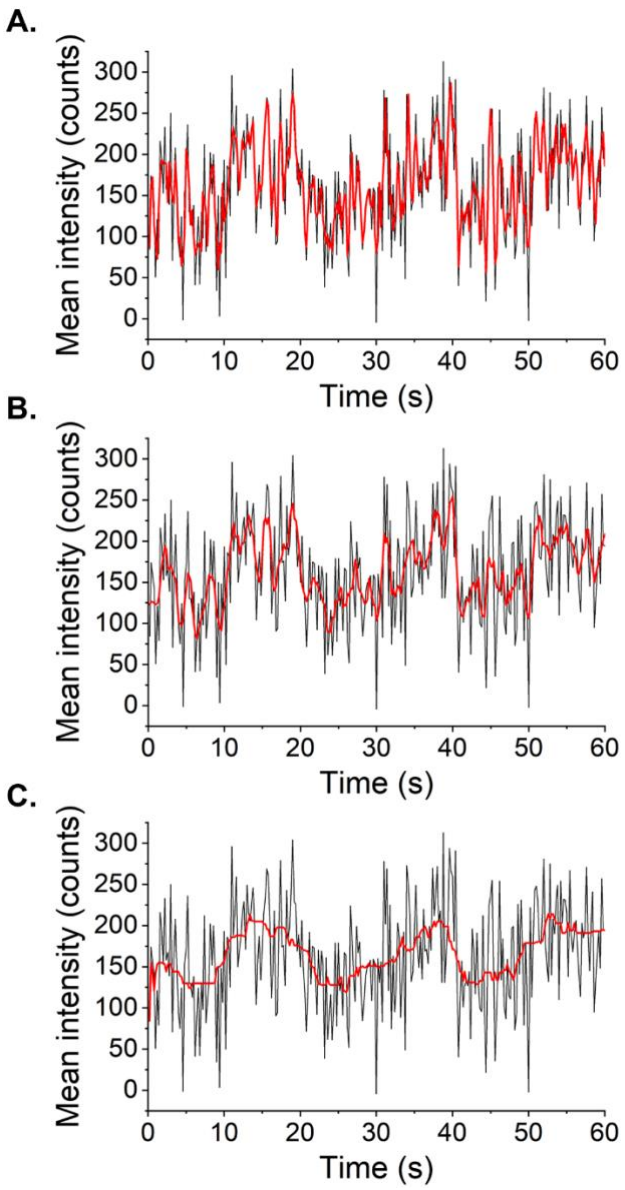

Figure S9. Background-subtracted fluorescence signals from a representative single pore shown in Figure 4D with data smoothing by Savitzky-Golay filter (*red*) using a 3rd order polynomial fit with 5 (A), 10 (B), and 25 (C) points.

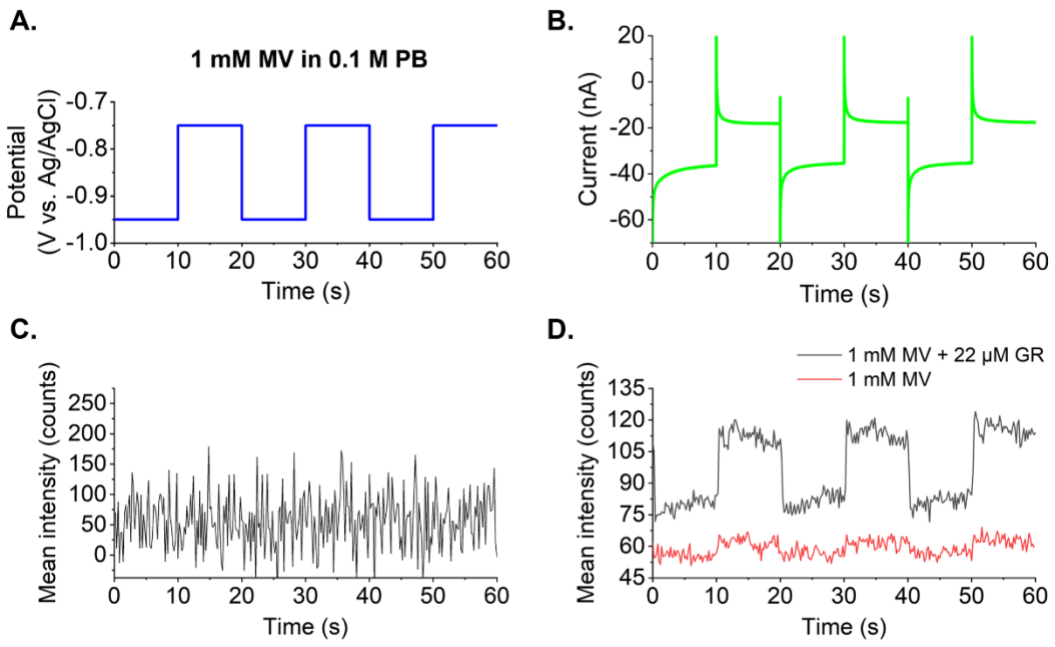

Figure S10. Spectroelectrochemical response of 1mM MV in 0.1 M PB in E-ZMWs in the absence of GR. **A**. Step potential-time plot. **B**. Current response. **C**. Representative fluorescence trajectories under step-potential perturbation obtained from a single pore. **D**. Average fluorescence signals from 350 pores with and without GR under step-potential perturbation.

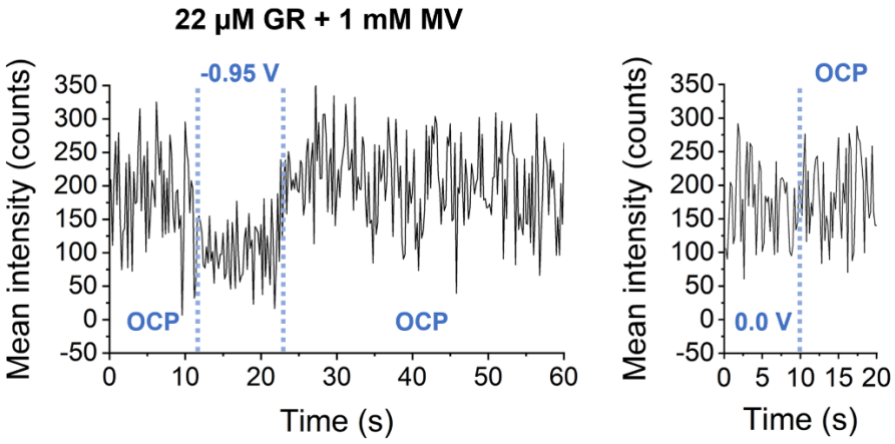

Figure S11. Representative fluorescence response obtained from a single nanopore, containing 22 µM GR and 1 mM MV in 0.1 M PB solution, upon applying either a reducing (*left*) or oxidizing (*right*) potential, *i.e.* –0.95 V or 0.0 V for 10 s in the middle of a time window for which the potential was otherwise held at open circuit potential.